International Journal of Architectural, Civil and Construction Sciences
ISSN: 2415-1734
Vol:10, No:2, 2016

Seismic Fragility Assessment of Continuous Integral Bridge Frames with Variable Expansion Joint Clearances

P. Mounnarath, U. Schmitz, Ch. Zhang

***Abstract*—**Fragility analysis is an effective tool for the seismic vulnerability assessment of civil structures in the last several years. The design of the expansion joints according to various bridge design codes is almost inconsistent, and only a few studies have focused on this problem so far. In this study, the influence of the expansion joint clearances between the girder ends and the abutment backwalls on the seismic fragility assessment of continuous integral bridge frames is investigated. The gaps (ranging from 60 mm, 150 mm, 250 mm and 350 mm) are designed by following two different bridge design code specifications, namely, Caltrans and Eurocode 8-2. Five bridge models are analyzed and compared. The first bridge model serves as a reference. This model uses three-dimensional reinforced concrete fiber beam-column elements with simplified supports at both ends of the girder. The other four models also employ reinforced concrete fiber beam-column elements but include the abutment backfill stiffness and four different gap values. The nonlinear time history analysis is performed. The artificial ground motion sets, which have the peak ground accelerations (PGAs) ranging from 0.1 g to 1.0 g with an increment of 0.05 g, are taken as input. The soil-structure interaction and the P-Δ effects are also included in the analysis. The component fragility curves in terms of the curvature ductility demand to the capacity ratio of the piers and the displacement demand to the capacity ratio of the abutment sliding bearings are established and compared. The system fragility curves are then obtained by combining the component fragility curves. Our results show that in the component fragility analysis, the reference bridge model exhibits a severe vulnerability compared to that of other sophisticated bridge models for all damage states. In the system fragility analysis, the reference curves illustrate a smaller damage probability in the earlier PGA ranges for the first three damage states, they then show a higher fragility compared to other curves in the larger PGA levels. In the fourth damage state, the reference curve has the smallest vulnerability. In both the component and the system fragility analysis, the same trend is found that the bridge models with smaller clearances exhibit a smaller fragility compared to that with larger openings. However, the bridge model with a maximum clearance still induces a minimum pounding force effect.

***Keywords*—**Expansion joint clearance, fiber beam-column element, fragility assessment, time history analysis.

I. Introduction

HIGHWAY bridges are essential infrastructures in transportation systems in the European and other regions. These structures should be designed to survive both normal and seismic situations. The restoration of these bridges should be performed with the minimum cost and time after an earthquake event to ensure the traffic flow and economy. Therefore, the design of bridges to attain these goals is still a challenge for civil engineers and researchers around the world. Although some design codes are available, such as Caltrans [1] and Eurocode 8-2 [2], but they are still inconsistent especially in the design of the expansion joint clearances. Some studies on the analysis and modeling of the expansion joints have been carried out so far. Kawashima and Penzien [3] examined the dynamic behavior and the seismic response of the bridge model by emphasizing the discontinuous behavior of the expansion joints. They also correlated their analytical study with the experimental response. Raheem [4] developed an analytical model for the expansion joints which takes into account of the interaction of the adjacent bridge segments and the impact effect. He also developed three kinds of restrainers and associated those with the expansion models for studying the mitigation of pounding and prevention of unseating at the opening joints of isolated multi-span bridges. Banerjee and Shinozuka [5] analyzed the continuous integral bridge frame by including the modeling of a simplified gap element for pounding at the expansion joint of the middle girder span and by adding a hook element for restrainers at that expansion joint. The gap elements for pounding at the abutments were also included. However, only one design gap value for pounding at the abutments was investigated. Mitoulis [6] analyzed three real bridge models with the variations of the total lengths, the clearances at the expansion joints, and the backfill models. He included the displacements of the girders in the design of the expansion joints as specified in Eurocode 8-2 [2]. However, the expansion joints were designed for only a specific earthquake level for each bridge. His analysis result still does not cover other cases with various ranges of the earthquake intensity levels and the verification of its consistency is still required.

Fragility analysis is an effective tool for the seismic vulnerability assessment of civil structures under various levels of the earthquake excitations. This technique is reliable, and can illustrate a clear trend of the structural behavior and the damage probability. It was applied by many researchers ([7]-[16], and etc.) to carry out the bridge analysis for various objectives so far. The response analysis of bridges with the inclusion of the abutment models mainly depends on the method of the modeling of the abutments and backfills as well

P. Mounnarath, Ph.D. candidate is with the University of Siegen, D-57068 Siegen, Germany (phone: +49-15211237295; e-mail: phonepheth.mounnarath@uni-siegen.de).

U. Schmitz, Prof. Dr. and Ch. Zhang, Prof. Dr. are with the Department of Civil Engineering, University of Siegen, D-57068 Siegen, Germany (e-mail: schmitz@bau.uni-siegen.de, c.zhang@uni-siegen.de).

as the design and modeling of the expansion joint clearances. Unfortunately, studies on these problems are still limited, especially for various ranges of the different input ground motions like the fragility analysis. Therefore, this study focuses on the seismic fragility assessment of continuous integral bridge frames by considering the influence of the expansion joint clearances on the modeling of the abutment backfill stiffness. The movement of the girders at openings is assumed to occur in many scenarios. For the first case, the girder is assumed to be freely moveable. For the second case, the girder is allowed to move to the finite value of the clearance that is designed for service actions only. The openings for the third, fourth, and fifth cases are designed for the consideration of the partial seismic displacements under the damage limitation, collapse prevention, and extra earthquake levels, respectively. Detailed information can be found in the next sections.

II. Bridge Properties and Parameters

A. Bridge Properties

A continuous integral bridge frame with four spans is considered in this study as a prototype bridge as shown in Fig. 1. The clear height of all piers is taken as 30 m and their sectional properties are designed similarly in order to provide uniform vertical and lateral stiffness. The initial geometrical design of all structural members is then carried out. The girder and piers are designed by using the concrete classes C35/45 and C30/37 according to Eurocode 2 [17], respectively. The reinforcing steels of all structural components belong to the steel grade A706M of Caltrans [1], which has the characteristic yield and ultimate strengths of 420 and 550 MPa, respectively. The pre-stressing steels utilize the steel grade Gr270 of Caltrans [1], which has the characteristic tensile strength of 1860 MPa. All detailed material properties can be further found in the specified references. The expected/mean material properties are assigned to each structural member in both linear and nonlinear analysis. The linear analysis is performed by using the response spectrum analysis method. Two seismic design levels with a PGA of 0.175 g and a PGA of 0.35 g are assigned and represented for the damage limitation and the collapse prevention levels, respectively. The bridge is designed as a ductile frame by following Eurocode 8-1 [18], Eurocode 8-2 [2], and Eurocode 2 [17] standard specifications. The behavior factors are taken as 3.5 for the two horizontal directions and 1 for the vertical direction. The bridge is assumed to be located on the soil type D with the importance factor equal to 1. Fig. 2 shows the sectional properties of the piers and the girder at the middle spans. Fig. 3 depicts the foundation plans of the three piers which are later used in the computation of the soil spring stiffness as illustrated in Table I.

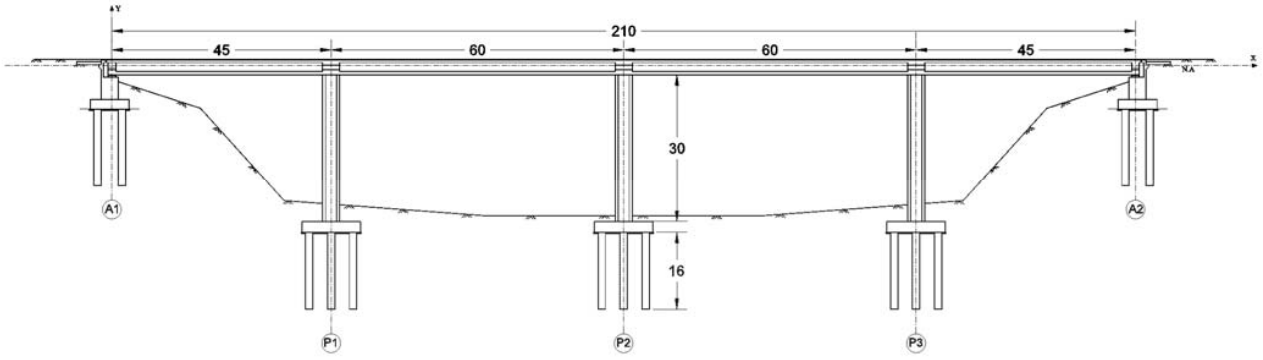

Fig. 1 Longitudinal profile of the prototype bridge (unit: [m])

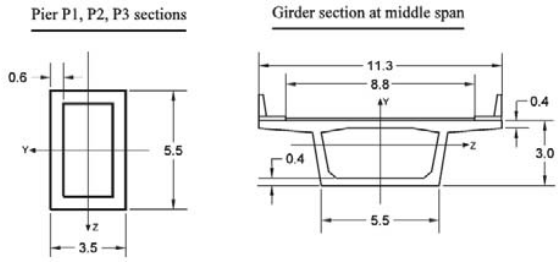

Fig. 2 Cross sections of the piers and the girder (unit: [m])

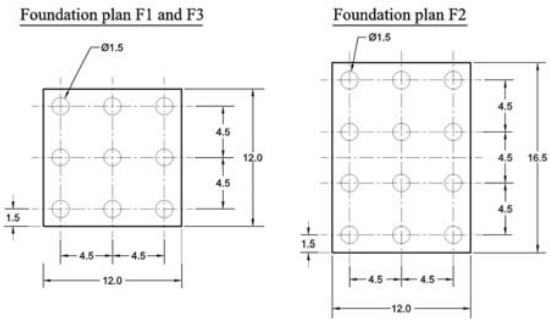

Fig. 3 Foundation plans of the three piers (unit: [m])

TABLE I
STIFFNESS VALUE OF THE SOIL SPRING ELEMENTS

No	Stiffness value	Unit	Pier P_1	Pier P_2	Pier P_3
1	K_x	kN/m	2.1×10^6	2.8×10^6	2.1×10^6
2	K_y	kN/m	4.9×10^6	6.5×10^6	4.9×10^6
3	K_z	kN/m	2.1×10^6	2.8×10^6	2.1×10^6
4	K_{rx}	kN.m/rad	2.5×10^7	3.3×10^7	2.5×10^7
5	K_{ry}	kN.m/rad	3.7×10^6	4.9×10^6	3.7×10^6
6	K_{rz}	kN.m/rad	2.5×10^7	3.3×10^7	2.5×10^7

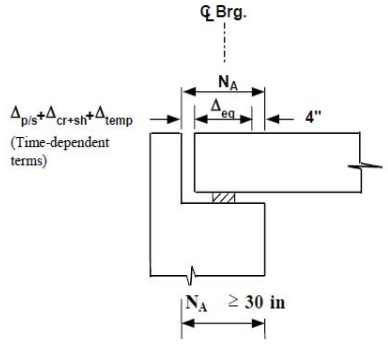

Fig. 4 Abutment seat width requirements in Caltrans [1]

B. Design of the Expansion Joint Clearances

The design of the expansion joints by various bridge design codes such as Caltrans [1], Eurocode 8-2 [2]; is almost inconsistent. Caltrans [1] accounts for only the serviceability effects as shown in Fig. 4. Where $\Delta_{p/s}$ is the displacement attributed to the pre-stress shortening, Δ_{cr+sh} is the displacement attributed to the creep and shrinkage, and Δ_{temp} is the displacement attributed to the thermal expansion and contraction. Whereas Eurocode 8-2 (section 2.3.6.3) [2] accounts for the partial fraction of the seismic displacement from the linear analysis to the calculation of the required clearances of the expansion joints as given by

$$d_{Ed} = d_E + d_G + \psi_2 d_T , \quad (1)$$

where d_G is the long-term displacement due to permanent and quasi-permanent actions (e.g. post-tensioning, shrinkage and creep for concrete girders). For simplicity, in this context, this term is computed by assuming that it is equivalent to the thermal contraction at the temperature of 30°C ([19] and [6]). d_T is the displacement due to thermal expansion (here, it is computed by assuming a temperature of 25°C), ψ_2 is the combination factor for the quasi-permanent value of the thermal action (0.5). In (1), d_E is the design seismic displacement determined

$$d_E = \pm\eta\mu_d d_{Ee} , \quad (2)$$

where η is the damping correction factor that can be determined by

$$\eta = \sqrt{\frac{1}{(0.05+\xi)}} , \quad (3)$$

μ_d is the displacement ductility factor given by

$$\mu_d = q \qquad if\ \ T \geq T_0 = 1.25T_c , \quad (4)$$

$$\mu_d = (q-1)\frac{T_0}{T} + 1 \leq 5q - 4 \qquad if\ \ T < T_0 , \quad (5)$$

and d_{Ee} is the seismic displacement computed from the linear elastic analysis (response spectrum analysis). In (3)-(5), ξ is the damping ratio (taken equal to 0.05 in this study), q is the behavior factor, T is the fundamental period in the considered horizontal direction, and T_c is the corner period defined in the response spectrum curve.

Section 2.3.6.3 (5) of Eurocode 8-2 [2] allows using an appropriate fraction of the design seismic displacement and the thermal expansion for the non-critical structural components (e.g. girder movement joints and abutment backwalls). In this study, we apply the recommended values by the code, which are 40% for the design seismic displacement and 50% for the thermal expansion in (1). It could be found from the response spectrum analysis that the required expansion joint clearance between the girder and abutment backwalls is approximately 0.06 m computed by following Caltrans's procedure. And it is about 0.15 m and 0.25 m for satisfying the two design earthquake levels (damage limitation and collapse prevention, respectively) computed by following Eurocode 8-2 [2]. However, to set sufficient parameters, a larger opening value with 0.35 m is supplemented as an extra value as listed in Table II.

TABLE II
MAIN PARAMETERS OF THIS STUDY

No	Earthquake levels	Clearances (m)	Codes
1	All	0.06	Caltrans
2	0.175 g	0.15	Eurocode 8-2
3	0.35 g	0.25	Eurocode 8-2
4	Extra	0.35	-

III. FRAGILITY ANALYSIS PROCEDURE

A. Structural Modeling

The detailed nonlinear structural modeling and analysis are performed in OpenSees [20]. The three-dimensional skeleton beam-column elements are modeled as shown in Fig. 5. Two main types of total five structural models are analyzed and compared. The first model as depicted in Fig. 5 (a) serves as a reference. This model uses simplified restraints at both ends of the girder as shown in Fig. 7 (a). The vertical flexibility of the abutments and bearings is neglected. The simplified vertical restraints replace those effects. The girder is allowed to move freely in the longitudinal direction. The longitudinal torsion is assumed to be perfectly restrained using the transverse shear keys. The girder ends and the abutments are also assumed to be able to contact perfectly and move together in the transverse direction by the mechanism of the transverse shear keys and stoppers.

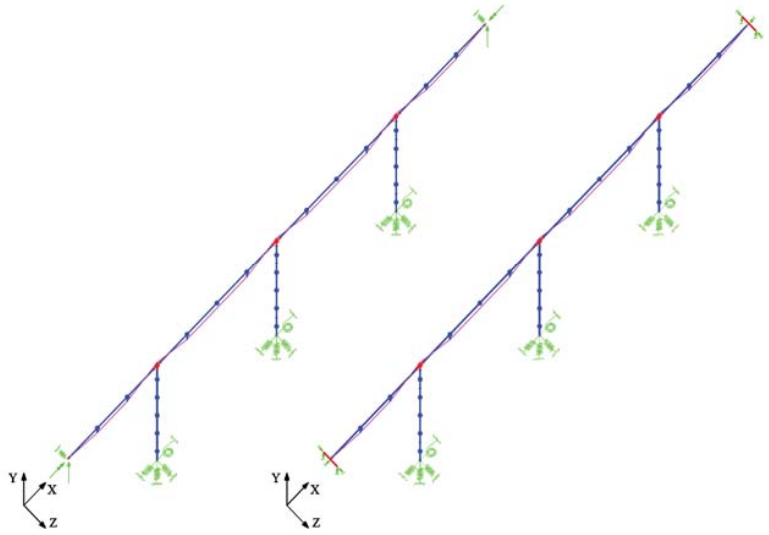

(a) (b)

Fig. 5 Skeleton beam-column element models: (a) reference model, (b) variable models

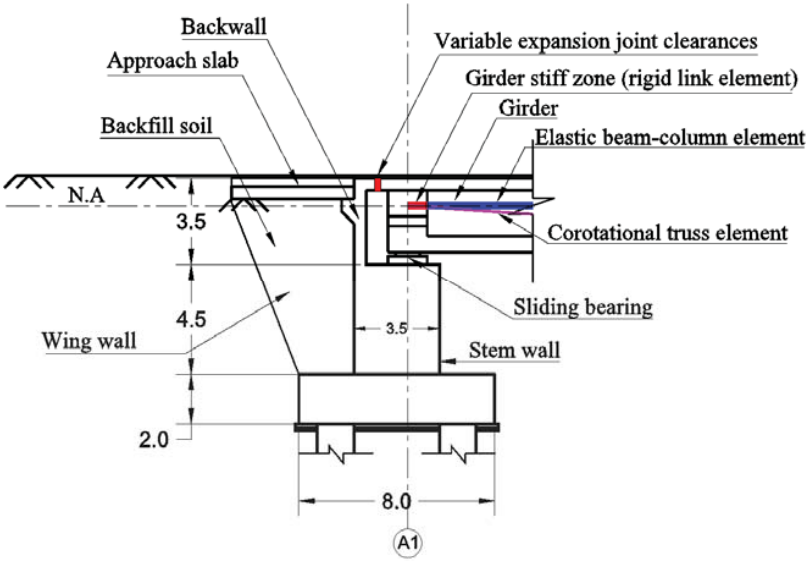

Fig. 6 South abutment and girder connection details

As it could be observed from the pushover analysis in SAP2000 [21] that the girder's plastic hinges are in the elastic range only, thus the modeling of the girders for all frame models in this study employs the elastic beam-column elements. The pre-stressing tendons in the reference and other models are represented by the Corotational truss elements in OpenSees [20] as shown in Figs. 6 and 7. The total tendon sectional area with Uniaxial Elastic Perfectly-Plastic Gap Material is assigned. Fig. 5 (b) illustrates the other four models, which are referred to as the variable models. The models consider the properties of the longitudinal and the transverse backfill stiffness. Four different values of the expansion joint clearances between the girder and the abutment backwalls are used as the main variables of the longitudinal backfill stiffness models as shown in Figs. 6-8. The modeling of the abutment sliding bearings is also included. The modeling of the longitudinal backfill stiffness at the south abutment (or passive direction) applies the Two Node Link Element with Uniaxial Elastic Perfectly-Plastic Gap Material as shown in Fig. 8 (a). The embankment fill material is assumed to meet the requirements of the Caltrans standard specifications [1]. The longitudinal backfill stiffness is calculated by

$$K_{abut} = K_i \times w_{bw} \times \left(\frac{h_{bw}}{1.7m} \right), \quad (6)$$

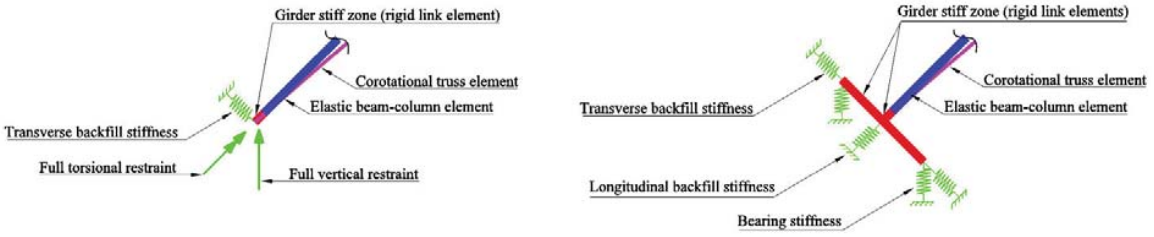

(a) (b)

Fig. 7 Girder-end supports: (a) reference model, (b) variable models

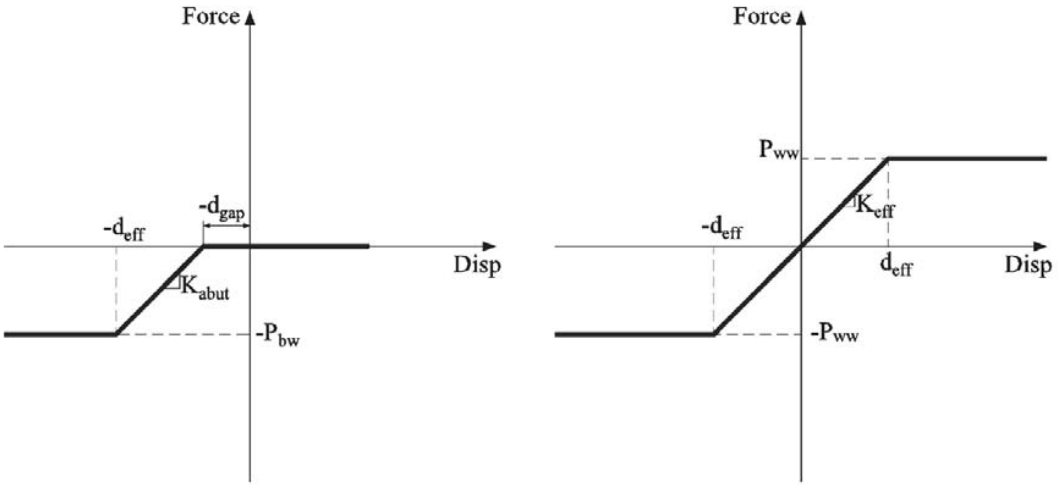

(a) (b)

Fig. 8 Backfill stiffness models: (a) longitudinal stiffness model, (b) transverse stiffness model

where K_i is the initial stiffness which is taken as 28.7 kN/mm/m. w_{bw} is the projected width of the backwall for the seat abutment, and h_{bw} is the height of the abutment backwall. The idealized bilinear force-displacement law can be determined by using

$$P_{bw} = A_e \times 239kPa \times \left(\frac{h_{bw}}{1.7}\right), \quad (7)$$

where A_e is the effective abutment wall area computed by

$$A_e = h_{bw} \times w_{bw}. \quad (8)$$

The transverse backfill stiffness is calculated similarly. Instead of using the Two Node Link Element, it is replaced by the Zero-Length Element with Uniaxial Elastic Perfectly-Plastic (without Gap) Material as illustrated in Fig. 8 (b). The idealized bilinear force-displacement law is determined by assuming the wing walls as diaphragm walls and adjusting factor 8/9 for considering the difference in the participation of both wing walls [1], [22]. However, this study focuses mainly on the longitudinal analysis and the transverse backfill stiffness has only very small or almost no influences on the analysis. The detailed procedure for computing that value will be not presented here, but it can be found in [1] and [22]. It should also be noted that the friction between the approach slabs and the backfill soil as well as the friction between the abutment wing walls and the surrounding soils are also neglected in this study. The sliding bearings are modeled by using Single Friction Pendulum Bearing Elements in OpenSees [20] and assigning the friction coefficient of 0.04. The effective radius of the concave sliding surface is taken as 3.6 m. The vertical stiffness is defined as 170000 kN/m. The properties of all sliding bearings are specified by the Manufacturer (Mageba Inc., USA [23]). The approximated horizontal yield displacement has been obtained by following the procedure of [24]. The stiff zones at both ends of the girders for all studied models are represented by rigid link elements as shown in Figs. 6 and 7. The elastic stiffness of these elements has been assigned to be about 100 times of their surrounding elements [25].

Fig. 9 shows the connection details of the pier, girder, and foundation at Pier P2. It can be seen that the flexibility of the pier foundation is considered, and it is modeled by using Zero-Length Elements with Uniaxial Elastic Material for representing all stiffness values in all six degrees of freedom. These values are listed in Table I. As can be seen from Fig. 9, several fiber beam-column elements are used to separate the potential plastic hinge zones and the outer zones. These two zones have different spacings of the lateral reinforcing steels

or the core concrete confinement factors. Five points of the Gauss-Lobatto integration per one element are applied. The lumped masses are distributed uniformly along the height of the piers and also along the length of the girder. It can be observed that the strain penetration lengths at both ends of the piers increase the height of the idealized fiber beam-column elements. Again, the rigid connection zones between the piers and the girders are modeled by using the rigid link elements similarly as stated earlier. Fig. 10 illustrates the typical fiber-reinforced concrete section of the piers in this study. The cover and the core concrete fiber patches are modeled by using the unconfined and confined concrete material model of Mander et al. [26] or the Concrete04 Material in OpenSees [20]. The steel layers are modeled by employing the Giufre-Menegotto-Pinto model [27] or the Steel02 Material in OpenSees [20].

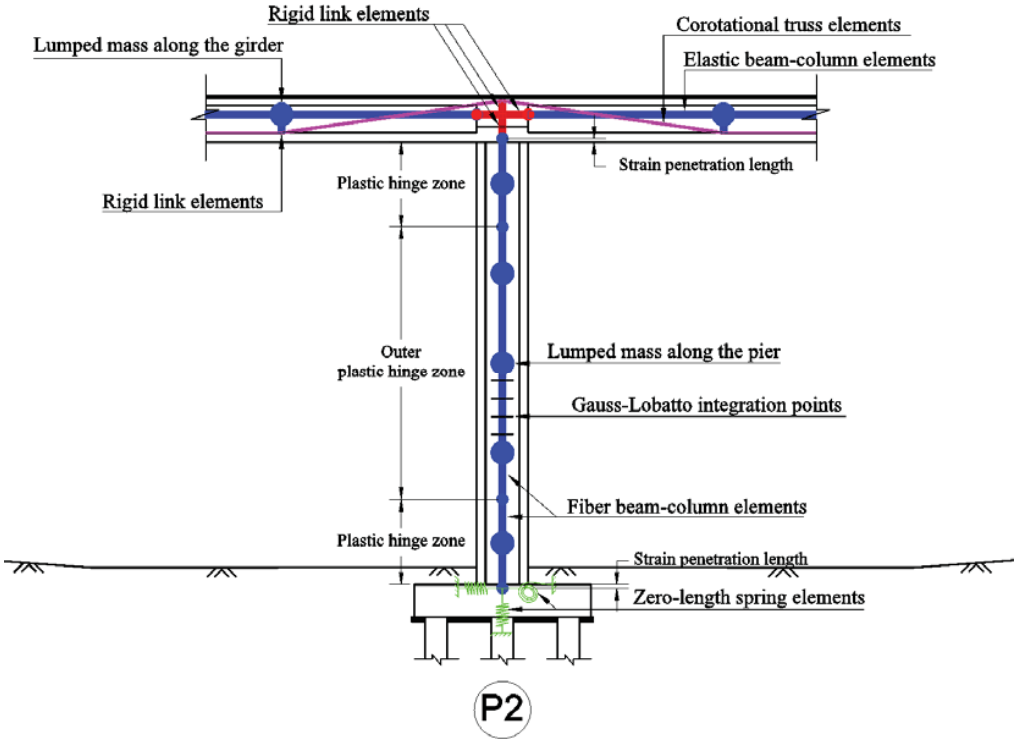

Fig. 9 Pier, girder, and foundation connection details

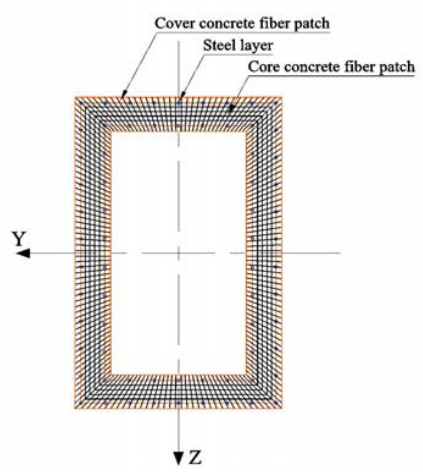

Fig. 10 Typical fiber-reinforced concrete section of the piers

B. Input Ground Motions

In this study, the artificial ground motion sets are taken as input. The accelerograms have been scaled to the target elastic acceleration response spectrum with a 5% damping ratio of Eurocode 8-1 [18] for the ground type D. The envelope shape of the computed curves is approximated by the Saragoni and Hart function [28]. The instant of time corresponding to a unitary density is taken to be 4 s and the value of the intensity corresponding to the last instant of time is set as 0.05 s. The input PGAs ranges from 0.10 g to 1.0 g with an increment of 0.05 g. The total duration of each ground motion is 20 s with a time-step of 0.005 s. The generation of these accelerograms has been achieved by employing the software SeismoArtif. v 2.1.0 (Seismosoft srl, Earthquake Engineering Software Solutions [29]). The built-in calculation method namely, the "Artificial Accelerogram Generation & Adjustment" is selected and applied. Fig. 11 shows the example of the elastic and generated response spectrum with a PGA of 0.35 g. The mean error between each generated curve and the reference target curve is less than 10% which satisfies the required criteria. Fig. 12 illustrates the seven achieved ground motions.

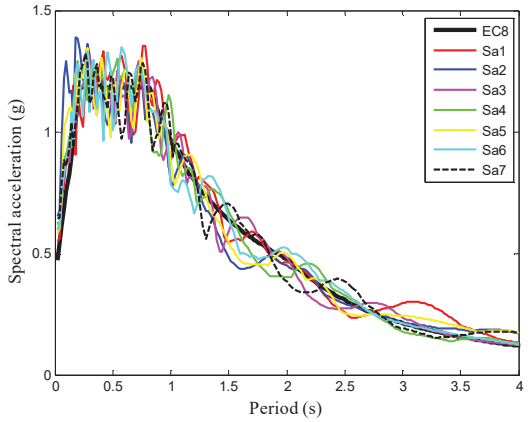

Fig. 11 Target elastic and generated response spectrum curves with a 5% damping ratio

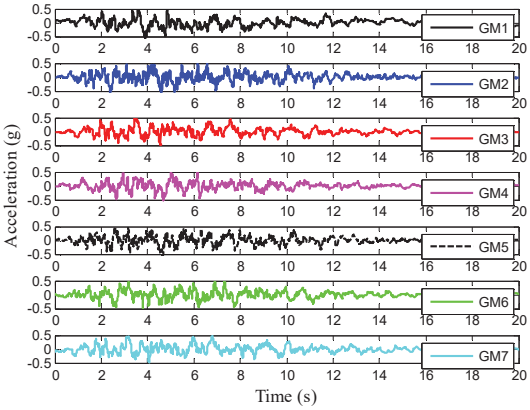

Fig. 12 Seven achieved ground motions with a PGA of 0.35 g

C. Nonlinear Time History Analysis (NTHA)

The static analysis of the idealized structural models under the gravity loads is firstly performed in OpenSees [20]. Then the constant gravity loads are maintained and the computed time is reset to zero before performing the dynamic analysis. Various dynamic analysis methods are recently developed and available. However, this study employs the well-known nonlinear time history analysis method. The time-step for the analysis is taken as 0.005 s, and the total duration of the analysis is set to be 35 s. This duration has been split into two portions. The first portion is about 20 s which is used for the analysis of the input ground motion. The second portion with 15 s is utilized for the free vibration analysis after ending the earthquake input data. The second portion is included to ensure the stop of the structural shaking. The time integration method employs the Hilber-Hughes-Taylor method. The main input parameter α is taken as 0.68 to ensure the unconditionally stable calculation. The Rayleigh damping is used for the mass-stiffness proportional damping. As mentioned previously, seven accelerograms are applied as input per one PGA level. An average of each maximum response has been obtained.

D. Engineering Demand Parameters (EPDs) and Damage States (DSs)

Various studies related to the analytical fragility analysis of the bridge structures have used different sets of the engineering demand parameters (EDPs) and the damage states (DSs). Basoz and Mander [7] used the drift limits for weak piers and displacement limits for weak bearings as EDPs with the definition of four damage states such as slight, moderate, extensive and complete damage states. Kowalsky [30] applied the concrete strain and steel strain limits of the columns as the EDPs with two damage states, serviceability and damage control. Hwang et al. [8] employed the displacement ductility as an EDP. They defined five damage states, e.g., no damage, slight/minor damage, moderate damage, extensive damage and complete damage. HAZUS (FEMA) [31] defined only five qualitative damage states. The damage ranges are similar to that in [8]. Liao and Loh [9] also applied the displacement ductility of the piers and the displacement limits of the bearings similar to [8]. However, instead of defining five damage states, they assigned only four damage states as specified by [7]. Choi et al. [10] employed several EDPs such as the displacement ductility of the columns, the displacements of the steel and expansion bearings, the displacements of the fixed and expansion dowels. They defined only four damage states like in [7]. Nateghi-A and Shahsavar [12] used the inelastic displacement ductility ratio and the Park-Ang damage function of the columns as the EDPs with four damage states. Avsar [15] defined EDPs by using the curvature ductility, the shear capacity of the columns and the cap beams as well as the girder unseating. They set three new damage limits corresponding to the structural limit states defined by Priestley et al. [22]. Banerjee and Shinozuka [5] defined an EDP from only one response like the threshold rotational ductility demand. They used five damage states like in [8]. Zhang et al. [32] applied the section ductility and the shear strain of the elastomeric bearings as EPDs with four damage states. It is clear from the previous studies that the definitions of the engineering demand parameters and the damage states were inconsistent which depend on the objectives, conditions, and assumptions of different researchers. Therefore, in this study, the curvature ductility of the piers and the displacements of the sliding bearings at the abutments are selected as two main EDPs. Four damage states as specified in [7] are used. Firstly, the displacement ductility capacity in the four DSs is determined according to the procedure of [8]; then it is converted to the curvature ductility capacity by applying the expression in [33] as

$$\mu_\phi = 1 + \frac{\mu_\Delta - 1}{\frac{3L_p}{L}(1 - 0.5\frac{L_p}{L})}, \quad (9)$$

where μ_ϕ is the curvature ductility capacity, μ_Δ is the displacement ductility capacity, L is the distance from the plastic joint to the point of zero moment in the piers, and L_p is the plastic hinge length estimated according to Eurocode 8-2 [2]

$$L_p = 0.1L + 0.015 f_{yk} d_s , \quad (10)$$

in which f_{yk} is the characteristic yield stress of longitudinal reinforcement (in MPa), and d_s is the longitudinal steel bar diameter.

The displacement capacity for the complete damage state of the sliding bearings is selected by using the design manual of the Reston Pendulum Sliding Bearing (Mageba Inc., USA [23]) and by the engineering judgment introduced by us. Other values for the first three damage states have adopted the capacity values of the expansion bearings applied by [10]. Table III lists the EDPS and the DSs in this study.

TABLE III
ENGINEERING DEMAND PARAMETERS AND DAMAGE STATES

No	Damage states	Displacement ductility	Curvature ductility	Bearing displacement (mm)
1	Slight (DS1)	1.00	1.00	50
2	Moderate (DS2)	1.46	2.39	100
3	Extensive (DS3)	3.17	7.58	150
4	Complete (DS4)	6.17	16.67	200

E. Component Fragility Analysis

Previous studies on seismic fragility analysis in last decades have applied various techniques to establish the fragility curves. In this study, the component fragility curves are computed by using the lognormal cumulative distribution function (cdf). This function can be derived by integrating the probability density function (pdf). The damage probability function can be calculated by

$$P_f = P\left[\frac{S_d}{S_c} \geq 1\right], \quad (11)$$

where P_f is the damage probability at a specific damage state, S_d is the structural demand, and S_c is the structural capacity.

Alternatively, (11) can be re-written in another form as

$$P_f = \Phi\left[\frac{\ln(S_d / S_c)}{\beta}\right], \quad (12)$$

where Φ [x] is the standard normal distribution function, and β is the logarithmic standard deviation or dispersion.

Based on the above principle, the first component fragility curves are then established in terms of the curvature ductility demand to the capacity ratio of the piers. The second component fragility curves are generated in terms of the displacement demand to the capacity ratio of the abutment sliding bearings. Fig. 13 (a) shows the pier fragility curves for the first variable structural model with the expansion joint clearance of 60 mm. Fig. 13 (b) presents the bearing fragility curves for the same model.

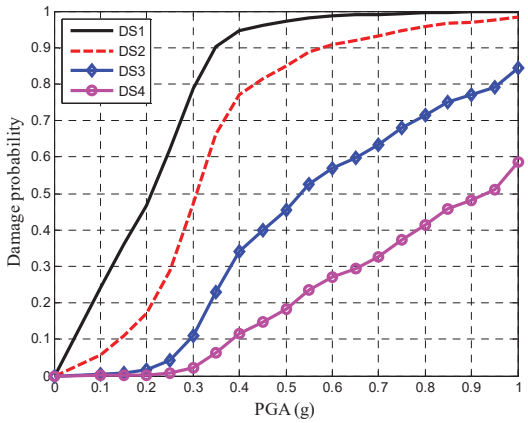

(a)

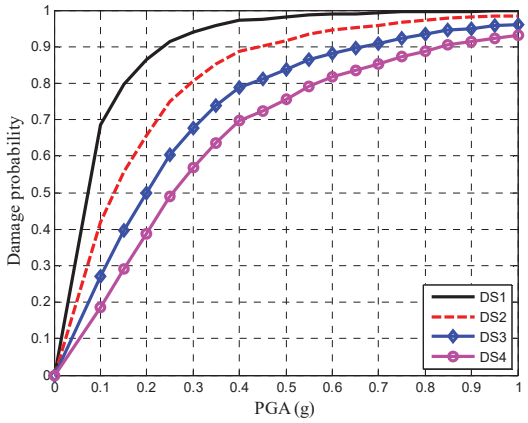

(b)

Fig. 13 Component fragility curves for the first variable structural model: (a) pier fragility curves, (b) bearing fragility curves

Fig. 14 illustrates the comparison of the pier fragility curves for the reference and other four variable bridge models with different expansion joint clearances ranging from 60 mm to 350 mm. It can be observed from all damage states (a) to (d) that the reference model exhibits a severe vulnerability compared to that of other models. The bridge models with smaller clearances exhibit a lower fragility compared to that with larger openings. The similar trend can be found in the bearing fragility curves as shown in Fig. 15.

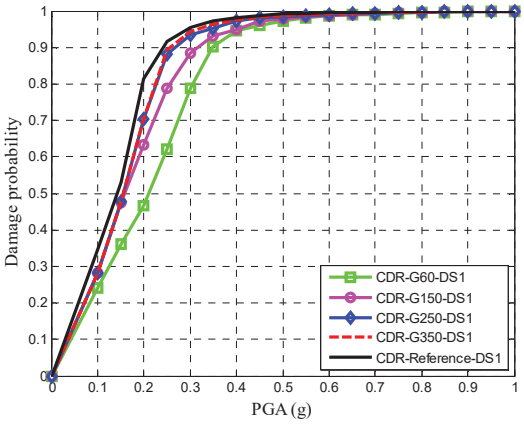

(a) Damage state 1 (DS1)

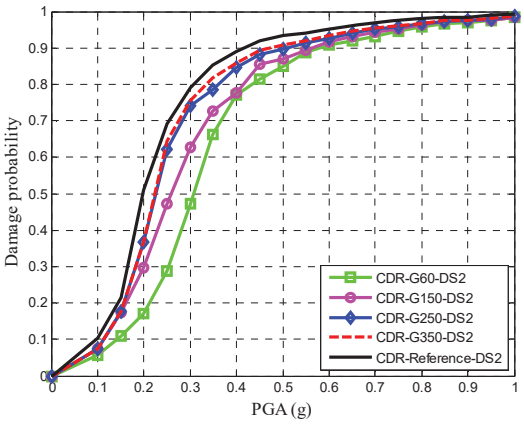

(b) Damage state 2 (DS2)

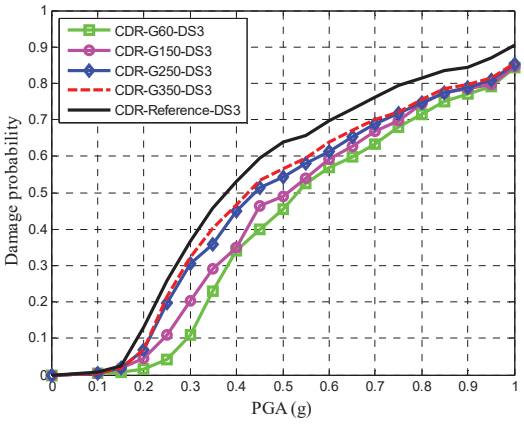

(c) Damage state 3 (DS3)

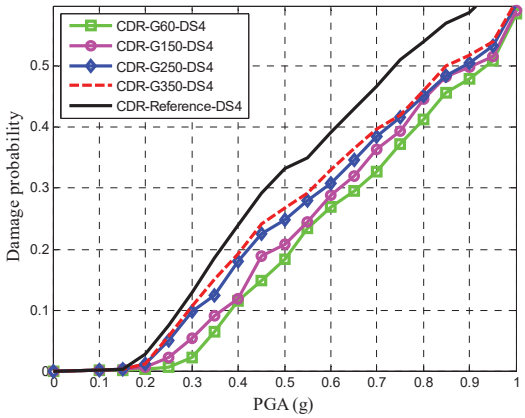

(d) Damage state 4 (DS4)

Fig. 14 Comparison of the pier fragility curves for all models

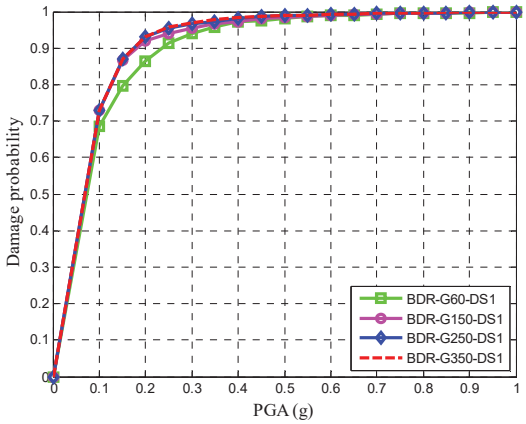

(a) Damage state 1 (DS1)

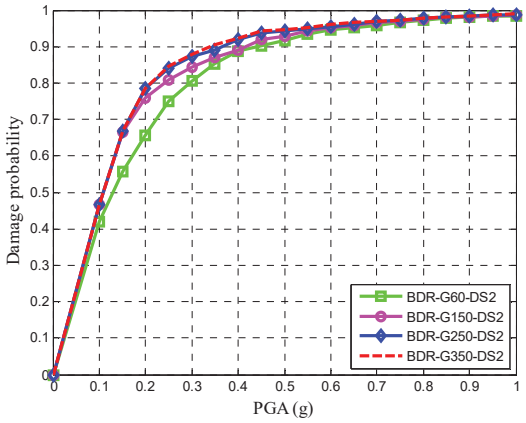

(b) Damage state 2 (DS2)

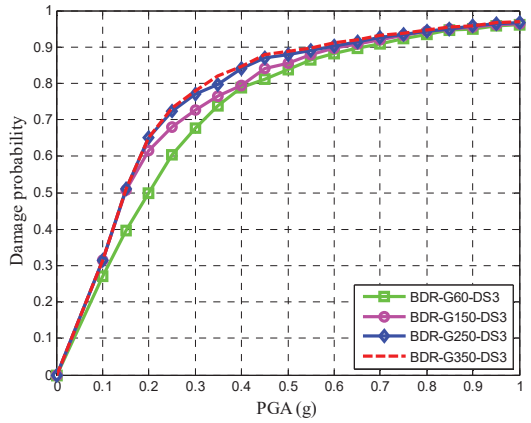

(c) Damage state 3 (DS3)

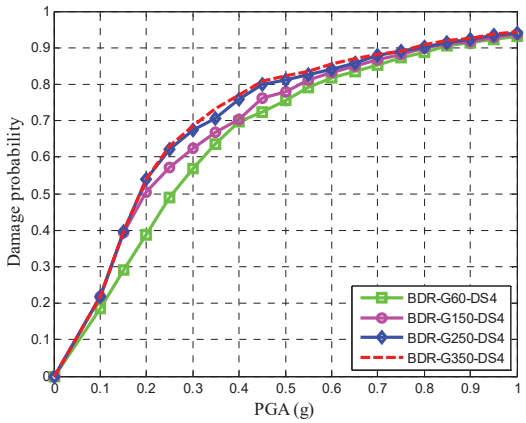

(d) Damage state 4 (DS4)

Fig. 15 Comparison of the bearing fragility curves for the four variable models

F. System Fragility Analysis

Previous studies have applied several different methods to determine the system fragility curves. Banerjee and Sinozuka [5] considered only the threshold rotational ductility demand as the main response to generate the fragility curves and utilized them as the system curves. Nateghi-A and Shahsavar [12] also employed only the responses from the piers to generate the fragility curves. Choi et al. [10] applied the first-order reliability theory to obtain the system fragility curves by combining various component fragility curves. Nielson and DesRoches [13] also developed the system fragility curves from the component curves as in [10]. However, they utilized the Monte Carlo simulation instead of the first-order reliability theory. Mackie and Stojadinovic [34] suggested determining the system fragility curves from the functionality and the post-earthquake retrofit cost. Zhang et al. [32] proposed a composite damage state. They used a proportion ratio 0.75 for columns and 0.25 for isolation devices by weighting the importance for the load-carrying capacity of the relative components during the earthquake and the post-earthquake repair cost. However, they used the proportion ratio for the first three damage states only. For the fourth damage state, they applied the governing damage between the piers and the isolators. From our points of view, the numerical computation of the real system fragility is too complicated or even impossible. The failure consequence of each bridge component cannot be determined numerically in contrast to the experimental works. Moreover, the derivation of the system fragility curves should be distinguished for each type of the bridge system. In fact, the failure of the abutment sliding bearings in a continuous integral bridge might induce only a very small effect on the piers and the overall bridge. Therefore, in this study, the simplified numerical computation is performed by using the importance weighting. The first-order reliability theory is applied to generate the upper-bound curves. It can be seen from Fig. 16 that the upper bound curve is almost the same curve as the bearing fragility curve even though the piers in the above prototype bridge play a more important role for carrying both the weights and the seismic forces. This is one of the reasons why we believe that the results obtained from this theory are too conservative if we take them as the system fragility curves. The lower-bound curves take the pier fragility curves, because as stated above; the piers are weighted as more important than the bearings in this work. The component fragility curves (pier fragility curves) of the reference bridge model serve as the system curves since the modeling of the abutment bearings is not included as described previously. The system fragility curves of four variable bridge models are obtained by weighting the importance of the piers and the abutment bearings. Finally, the proportional contribution ratios equal to 0.75 and 0.25 (similar to [32]) are taken for the pier and the bearing fragility curves, respectively. It is important to note that the proportions are specified in the fragility curves for all four damage states instead of only the first three damage states as in [32]. The upper bound fragility values are computed by

$$\max_{i=1}^{m}[P(F_i)] \le P(F_{upper}) \le 1-\prod_{i=1}^{m}[(1-P(F_i)], \quad (13)$$

where $P(F_{upper})$ is the damage probability of the upper bound values, and $P(F_i)$ is the damage probability of each component.

Fig. 17 shows the system fragility curves for all structural models. It can be seen from Figs. 17 (a) and (b) for the first and second damage states that at the PGA ranging from 0 to 0.15 g the fragility curves of the reference model exhibit a lower vulnerability compared to that of other models. After that range, the reference curves show a higher fragility compared to other curves. For the third damage state in Fig. 17 (c), the reference curve shows the smallest damage probability at the PGA levels smaller than 0.2 g. Moreover, at the PGAs ranging from 0.2 to 0.5 g, the reference curve still depicts a slight damage probability compared to that of the third and fourth variable bridge models with opening values of 250 and 350 mm, respectively. However, at the PGAs larger than 0.5 g it shows a severe vulnerability compared to other curves. In Fig. 17 (d), the reference curve show a lower fragility compared to that of all other bridge models. It can be observed

from Figs. 17 (a)-(d) that the bridge models with smaller clearances still exhibit a slighter failure probability compared to that with larger openings.

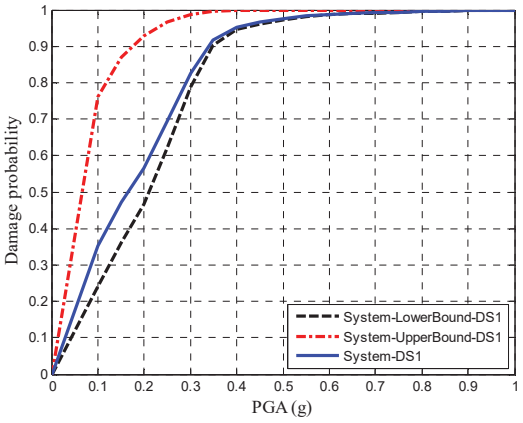

(a) Damage state 1 (DS1)

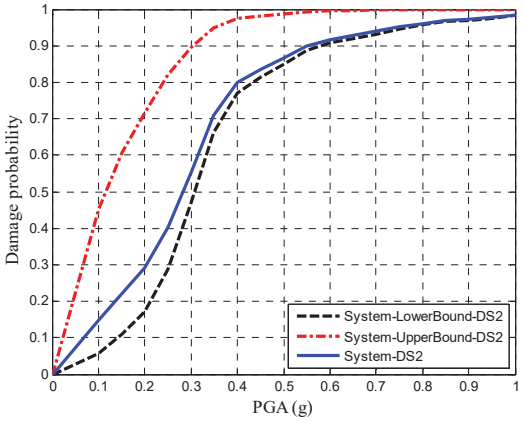

(b) Damage state 2 (DS2)

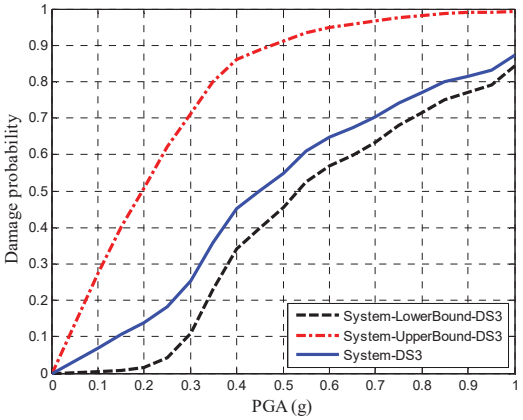

(c) Damage state 3 (DS3)

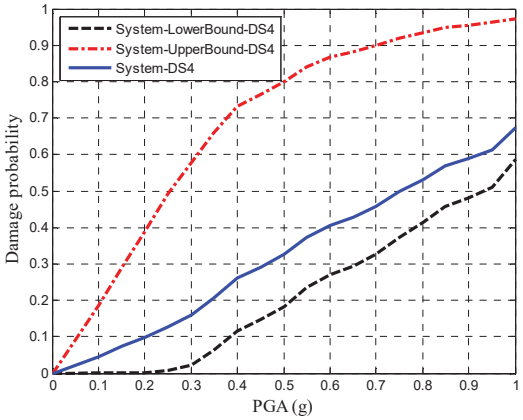

(d) Damage state 4 (DS4)

Fig. 16 System fragility curves for the first variable model

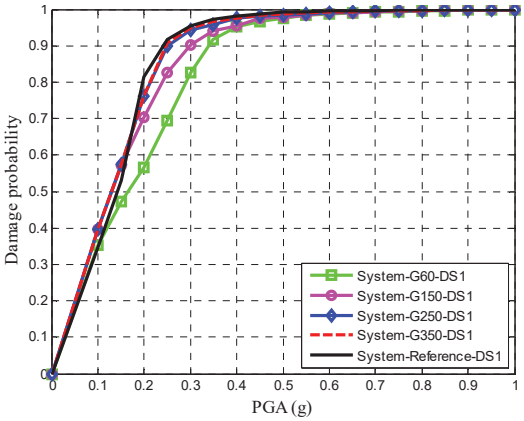

(a) Damage state 1 (DS1)

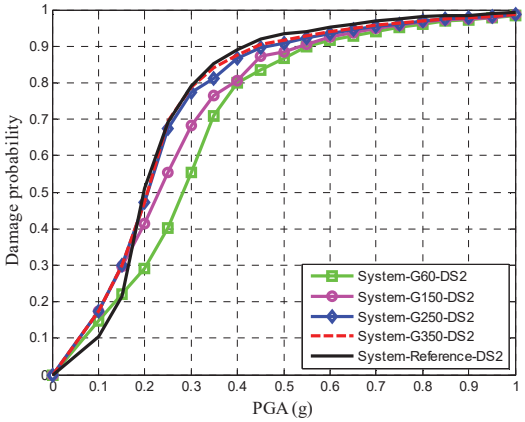

(b) Damage state 2 (DS2)

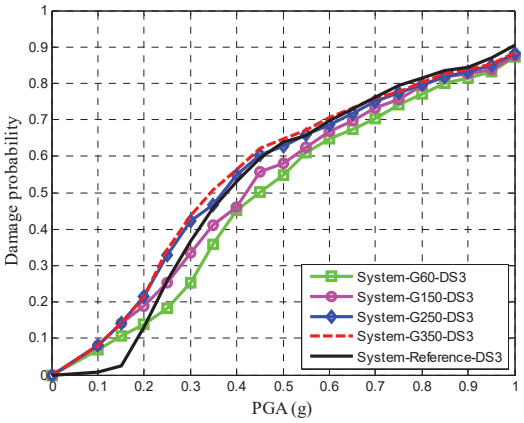

(c) Damage state 3 (DS3)

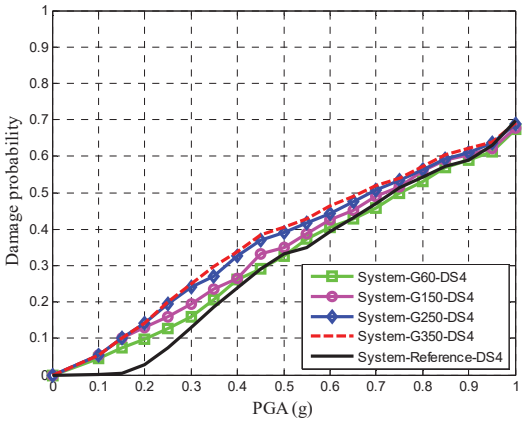

(d) Damage state 4 (DS4)

Fig. 17 System fragility curves for all bridge models

Fig. 18 shows the induced pounding force effect between the girder and the abutment backwalls. As expected, the bridge model with a maximum clearance induces a minimum pounding force effect.

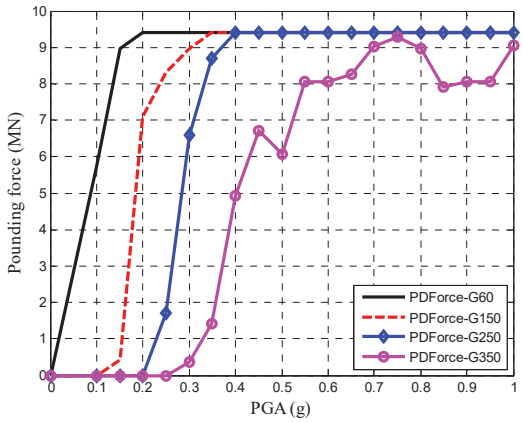

Fig. 18 Induced pounding force effect between the girder and the abutment backwalls

III. Conclusions

In this study, the seismic fragility assessment of continuous integral bridge frames with a simplified reference model and four variable bridge models with different expansion joint clearances and backfill stiffness is presented. The results can be concluded as follows:

- In the component fragility analysis, the reference model exhibits a severe vulnerability compared to that of other sophisticated models. The bridges with smaller clearances show a lower fragility compared to that with large openings. This verifies that the inclusion of the backfill stiffness in the modeling of variable bridge models can greatly reduce the responses of the superstructure, bearings, and piers. The bridge models with smaller clearances contribute more to the effective backfill resistances compared to that with larger gaps.
- In the system fragility analysis; for the damage states 1-3, the reference model shows a smaller damage probability at the lower PGA level. Then it exhibits a higher fragility compared to that of other variable bridge models. In the damage state 4, the reference curve has the lowest vulnerability, because the modeling of the abutment bearings is not included. The same trend can be found in the system fragility curves. The bridge models with larger openings possess a higher damage probability compared to that with smaller clearances.
- The result of the pounding effect shows that the bridge model with a larger clearance induces a smaller pounding force effect.
- Although the design of the expansion clearances by following the Caltrans's procedure in this study seems to be more practical compared to the method of Eurocode 8-2. However, the possible damages induced by the higher pounding force effects should be also taken into account, which is neglected in this study.

Acknowledgments

The first author acknowledges the financial support from the German Academic Exchange Service (DAAD) under the funding no. ID-57076385 and the supports by the University of Siegen, Germany.

References

[1] Caltrans, *Seismic Design Criteria Version 1.7*. California Department of Transportation, CA: Sacramento, 2013.
[2] Eurocode 8, *Design of Structures for Earthquake Resistance, Part 2: Bridges.* Brussels: European Standard EN 1998-2:2005, 2005.
[3] K. Kawashima, and J. Penzien, "Theoretical and experimental dynamic behavior of a curved model bridge structures," *Earthquake Engineering and Structural Dynamics*, vol. 7, pp. 129-145, 1979.
[4] S. E. A. Raheem, "Pounding mitigation and unseating prevention at expansion joints of isolated multi-span bridges," *Engineering Structures*, vol. 31, pp. 2345-2356, 2009.
[5] S. Banerjee, and M. Shinozuka, "Nonlinear static procedure for seismic vulnerability assessment of bridges," *Computer-Aided Civil and Infrastructure*, vol. 22, pp. 293-305, 2007.
[6] S .A. Mitoulis, "Seismic design of bridges with participation of seat-type abutments," *Engineering Structures*, vol. 44, pp. 222-233, 2012.

[7] N. Basoz, and J. Mander, *Enhancement of the Highway Transportation Lifeline Module in HAZUS*. National Institute of Building Sciences, 1999.
[8] H. Hwang, J. B. Liu, and Y. H. Chiu, *Seismic Fragility Analysis of Highway Bridges*. Report No. MAEC RR-4, Center for Earthquake Research Information, 2001.
[9] W. I. Liao, and C. H. Loh, "Preliminary study on the fragility curves for highway bridges in Taiwan," *Journal of the Chinese Institute of Engineers*, vol. 27, no. 3, pp.367-375, 2004.
[10] E. Choi, R. DesRoches, and B. Nielson, "Seismic fragility of typical bridges in moderate seismic zones," *Engineering Structures*, vol. 26, no. 2, pp. 187-199, 2004.
[11] E. Choi, J. Park, S.-J. Yoon, D.-H. Choi and C. Park, "Comparison of seismic performance of three restrainers for multiple-span bridges using fragility analysis," *Nonlinear Dyn.*, vol. 61, pp. 83-99, 2010.
[12] F. Nateghi, and V. L. Shahsavar, "Development of fragility and reliability curves for seismic evaluation of a major prestressed concrete bridge," in *Proc. 13th World Conference on Earthquake Engineering*, Vancouver, B.C. Canada, 2004, Paper No. 1351.
[13] B. G. Nielson, "Analytical fragility curves for highway bridges in moderate seismic zones," Ph.D. Thesis, Georgia Institute of Technology. Atlanta, Georgia, 2005.
[14] B. G. Nielson, and R. DesRoches, "Seismic fragility methodology for highway bridges using a component level approach," *Earthquake Engineering and Structural Dynamics*, vol. 36, pp. 823-839, 2006.
[15] Ö. Avsar, "Fragility based seismic vulnerability assessment of ordinary highway bridge in Turkey," Ph.D. Thesis, Middle East Technical University. Ankara, Turkey, 2009.
[16] M. S. Alam, M. A. R. Bhuiyan, and A. H. M. M Billah "Seismic fragility assessment of SMA-bar restrained multi-span continuous highway bridge isolated by different laminated rubber bearings in medium to strong seismic risk zones," *Bull Earthquake Eng.*, vol. 10, pp. 1885-1909, 2012.
[17] Eurocode 2, *Design of Concrete Structures, Part 1-1: General Rules and Rules for Buildings*. Brussels: European Standard EN 1992-1-1:2004, 2004.
[18] Eurocode 8, *Design of Structures for Earthquake Resistance, Part 1: General Rules, Seismic Actions, and Rules for Buildings.* Brussels: European Standard EN 1998-1:2003, 2003.
[19] PCI, Precast, *Prestressed Concrete Bridges, the High Performance Solution*. Comprehensive Bridge Design Manual, http://www.pci.org/publications/bridge, Accessed: 01/12/2014.
[20] OpenSees, *Open System for Earthquake Engineering Simulation, Version 2.4.6*, Pacific Earthquake Engineering Research Center, http://opensees.berkeley.edu/, Accessed: 23/09/2015.
[21] Computers and Structures, Inc. *SAP2000 Nonlinear, Version 17.2.0*. Structural Analysis Program, CA: Berkeley, 2015.
[22] M. J. N. Priestley, F. Seible, and G. M. Calvi, *Seismic Design and Retrofit of Bridges*. New York: John Wiley & Sons, Inc., 1996.
[23] Technical Manual, *Reston Pendulum Curved Surface Slider*. Mageba Seismic Protection Devices for Reliable Preservation of Structures, Mageba Inc., USA, 2015.
[24] M. C. Constantinou, P. Tsopelas, A. Kasalanati, and E. D Wolff, *Property Modification Factors for Seismic Isolation Bearings*. Multidisciplinary Center for Extreme Events Research, Technical Report MCEER-99-0012, Buffalo, New York, 1999.
[25] C. Casarotti and R. Pinho, "Seismic response of continuous span bridges through fiber-based finite element analysis," *Earthquake Engineering and Engineering Vibration*, vol. 5, no. 1, pp. 119-131, 2006.
[26] J. B. Mander, M. J. N. Priestley, and R. Park, "Theoretical stress-strain model for confined concrete," *ASCE J. Structural Eng.*, vol. 114, no. 8, pp. 1804-1825, 1988.
[27] M. Menegotto, and P. E. Pinto, *Method of Analysis of Cyclically Loaded RC Plane Frames Including Changes in Geometry and Non-elastic Behavior of Elements Under Normal Force and Bending*. Preliminary Report IABSE, No. 13, 1973, pp.15–22.
[28] G. R. Saragoni, and G. C. Hart, "Simulation of Artificial Earthquakes," *Earthquake Engineering and Structural Dynamics*, vol. 2, pp. 249-267, 1974.
[29] Seismosoft srl, *SeimoArtif, Version 2.1.0*, Earthquake Engineering Software Solutions, http://www.seismosoft.com. Accessed: 01/08/2014.
[30] M. J. Kowalsky, "Deformation limit states for circular reinforced concrete bridge columns," *ASCE J. Structural Eng.*, vol. 126, no. 8, pp. 869-878, 2000.
[31] HAZUS-MH MR1, *Technical Manual, Vol. Earthquake Model*. Washington DC: Federal Emergency Management Agency (FEMA), 2003.
[32] J. Zhang, Y. Huo, S.J Brandenberg, and P. Kashighandi, "Evaluation effectiveness and optimum design of isolation devices for highway bridges using the fragility function method," *Engineering Structures*, vol. 31, pp. 1648-1660, 2009.
[33] Federal Highway Administration (FHWA), *Seismic Retrofitting Manual for Highway Bridges*. Report No. FHWA-RD-94-052, VA: McLean, 1995.
[34] K. Mackie, and B. Stojadinović, "Performance-based seismic bridge design for damage and loss limit States," *Earthquake Engineering and Structural Dynamics*, vol. 36, no. 13, pp. 1953-1971, 2007.